This is a repository copy of *An investigation into the contact between soft elastic and poroelastic bodies rotating under load*.

Article:

de Boer, G orcid.org/0000-0002-5647-1771, Hewson, R, Bryant, M orcid.org/0000-0003-4442-5169 et al. (1 more author) (2017) An investigation into the contact between soft elastic and poroelastic bodies rotating under load. Tribology - Materials, Surfaces & Interfaces, 11 (4). pp. 193-201. ISSN 1751-5831

https://doi.org/10.1080/17515831.2017.1378852

An investigation into the contact between soft elastic and poroelastic bodies rotating under load

GN de Boer[1*], RW Hewson[2], MG Bryant[1], D Dowson[1]

Tribology – Materials, Surfaces & Interfaces: Special Issue on Soft Tribology

[1] School of Mechanical Engineering, University of Leeds, Woodhouse Lane, Leeds, LS2 9JT, UK

[2] Department of Aeronautics, Imperial College London, South Kensington Campus, London, SW7 2AZ, UK

[*] Corresponding author. Email: G.N.deBoer@leeds.ac.uk; Tel: +44(0)113 343 2220.

Abstract

This paper explores the contact of soft elastic and poroelastic bodies rotating under load and inspects the differences in load carrying capacity between the two types of material. Both materials have been widely used to describe the behaviour of biological systems such as articular cartilage in mammalian joints, however we demonstrate here that there are fundamental differences between the responses generated in which the poroelastic response has an additional fluid contribution to the solid structural response. In order to produce the same load carrying capacity it is shown that the poroelastic material must deform more than an incompressible soft elastic material with the same stiffness and that the solid load generated by a poroelastic material is the same as a soft elastic material with a zero Poisson's ratio.

Keywords: Contact mechanics; Soft elasticity; Poroelasticity; Load carrying capacity.

1. Introduction

Soft tribological interfaces are frequently encountered in natural systems which have evolved over millennia. Such interfaces include those of the natural synovial joints encountered, for example, in mammalian knees and hips. Such systems have demonstrated ultra-low friction coefficients (0.002-0.006) [1] in operating conditions more typical of the boundary lubrication regime. A number of explanations have been proposed for such low friction and while there is not a universal agreement as to the mechanisms describing the lubrication of natural synovial joints, many of the general concepts are well accepted [2-5]. This includes describing the cartilage material as a porous matrix with a pressurised interstitial fluid, leakage out of the porous matrix to provide some load bearing capability and, more recently, the role of long chained molecules attached to the cartilage surface to provide an immobilised lubricious layer. The mechanisms by which the super-lubricity of biological materials functions has been explored historically by a number of authors who have conducted experiments on cartilage and use biphasic theories to describe the interactions observed [6-8]. Recent research has confirmed the ultra-low friction of cartilage in operation and discusses the so called tribological rehydration of synovial joints [9-11].

Poroelastic models such as the work of Biot [12] address many of the challenges of modelling such systems, but many still remain to be addressed as more realistic representations of the performance of cartilage are considered. The potential for poroelasticity to describe the phenomena observed in articular cartilage has been extensively explored [13, 14], such biphasic theories use a combination of finite deformation and porous flow to derive the constitutive equations for the solid stress and fluid pressure respectively. Findings from the development of the biphasic theory have demonstrated that a significant fluid pressure can be maintained so long as the contact moves to hydrated regions faster than the rate of leakage [15, 16]. Modelling the poroelastic lubrication mechanisms has been a considerable challenge, with the large deformation of the cartilage and changing permeability with compression, as well as numerical problems in obtained computational solutions being some of the challenges [17-19].

This work examines the role of the porous fluid in a simplified tribological system when compared to purely elastic contacting materials, the role of the fluid pressurisation and how it relates to the equivalent elastic material's compressibility are considered and compared. The load carrying capacity of soft elastic and poroelastic materials are investigated demonstrating a significant difference in the mechanisms by which they operate. The model introduces an Eulerian frame of reference in in which two poroelastic faced bearings rotate under load, this allows steady compression-sliding to be considered and the potential load carrying capacity of both the solid and fluid phases to be investigated. Contact mechanics are also considered at the interface between the two bodies under frictionless conditions, no flow is permitted across the interface and as such fluid is confined to each of the contacting bodies and dry conditions apply.

2. Theory

In this paper the contact between two rotating bodies is investigated, the case studies conducted analyse the following: (i) soft elastic contact; and (ii) poroelastic contact. The remainder of this section outlines the equations, parameters and assumptions which define each of these models.

2.1 Elastic Contact

In Figure 1a two elastic bodies with given inner $R_{1,i}, R_{2,i}$ and outer radii $R_{1,o}, R_{2,o}$ are rotating with angular velocities Ω_1, Ω_2 about their origins. Figure 1b illustrates that when the separation δ between the two bodies is reduced beyond zero they come into contact and are deformed such that there is no penetration. As a result the contacting region is defined in x by where y = 0 and in which the contact pressure is positive, outside this region the contact pressure is zero. Since the angular velocities of the bodies are constant the elastic deformation in contact can be calculated using steady-state assumptions in which the bodies are compressing and sliding against each other. The out-of-plane dimension z is assumed to be orders of magnitude larger than the remaining dimensions and therefore plane strain assumptions apply to the 2D structural model developed.
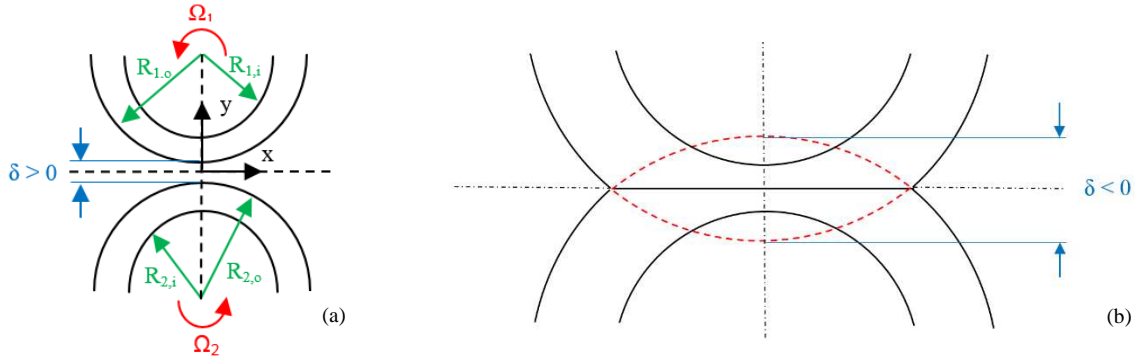

Figure 1 – (a) Schematic of two rotating bodies coming into contact, positive separation. (b) Close up view of the contacting region, negative separation.

Due to contact pressure, stresses are generated in the material and for which a linear elastic model is assumed to describe the structural behaviour of the material under load [20]. Such materials define that the stress-strain relationship is given by Eqs. (1)-(3). Deformation is therefore related to the material stresses by specifying a Young's modulus E and Poisson's ratio ν as material properties (see Eq. (4)). Where $\mathbf{u}$ is the deformation field, $\boldsymbol{\varepsilon}$ the strain tensor, $\boldsymbol{\sigma}$ the stress tensor, and μ, λ are the Lamé parameters. Elastic materials with a Poisson's ratio of $\nu = 0.5$ are considered incompressible since the volumetric contribution to stress dominates over the isochoric component, this is a well-established approach to modelling soft elastic materials which exhibit linear 'rubber-like' behaviour under load [21].

$$\nabla \cdot \boldsymbol{\sigma} = 0 \tag{1}$$

$$\boldsymbol{\sigma} = 2\mu\boldsymbol{\varepsilon} + \lambda \mathrm{tr}(\boldsymbol{\varepsilon})\mathbf{I} \tag{2}$$

$$\boldsymbol{\varepsilon} = \frac{1}{2}\left[\nabla\mathbf{u} + (\nabla\mathbf{u})^{\mathrm{T}}\right] \tag{3}$$

$$\mu = \frac{E}{2(1-\nu)} \qquad \lambda = \frac{E\nu}{(1+\nu)(1-2\nu)} \tag{4}$$

In order to solve for the solid elastic deformation the model is constrained using the following boundary conditions. Each of the contacting surfaces is allowed to freely deform until contact is reached, once contact is identified a frictionless Augmented Lagrangian approach is used to keep the surfaces from penetrating into each other [22]. This method applies a contact pressure at the interface which varies according to the magnitude of the

separation and is defined to cause a normal stress at the interface, such that $\mathbf{n} \cdot \boldsymbol{\sigma} = -p_c \mathbf{n}$ where p_c is the contact pressure. The penalty contact method is also capable of implementing the contact mechanics required, however this method was not selected because improved numerical stability was found using the Augmented Lagrangian approach. The remaining surfaces of the bodies are constrained by the separation such that the interface contacts about the line $y = 0$, for the upper body deformation is specified as $\mathbf{n} \cdot \mathbf{u} = \delta/2$ and for the lower body $\mathbf{n} \cdot \mathbf{u} = -\delta/2$ where the separation δ is negative in contact. This condition is implemented such that the boundaries are free to deform tangentially and is therefore consistent with the assumptions of steady compression-sliding at the contacting interface which arise from the constant values assigned to the rotational velocities of the bodies.

The load carrying capacity of the elastic contact $F_{elastic}$ is given by the integral of the contact pressure along the interface between the two bodies. This is described by Eq. (5) where s defines the arc length of the boundary $(ds)^2 = (dx)^2 + (dy)^2$, $\mathbf{n}$ is the boundary normal vector, F_{solid} is the solid load, and subscripts 1 and 2 represent integrals for each of the two bodies in contact. Because contact pressure is applied only where the two bodies intersect the solid material supports the total load applied at the interface, in the case of poroelasticity the fluid volume also contributes to the total load carrying capacity of the material as derived in Section 2.2.

$$F_{elastic} = F_{solid} = \int \|\mathbf{n} \cdot \boldsymbol{\sigma}\| \, ds_1 + \int \|\mathbf{n} \cdot \boldsymbol{\sigma}\| \, ds_2 \tag{5}$$

2.2 Poroelastic Contact

In contrast to elastic contact this section develops a poroelastic model in which the contacting bodies are no longer considered to be solid but rather biphasic in which pores in the solid material are filled with an interstitial fluid. For such a model the fluid flow in the porous media is described by Darcy's law and the solid deformation by a linear elastic relationship. Critically the coupling between these two phases is achieved by implementing a zero value for the material Poisson's ratio $\nu = 0$ and subsequently specifying a source term in the fluid flow equation related to volumetric strain. This ensures conservation of volume in both phases such that the change in volume due to solid deformation is equal to the volume of fluid exuded from the porous domain [12], this type of analysis is well-established for biphasic materials [13-17] as investigated in this article.

For the fluid phase Eq. (6) is derived from Darcy's law in order to describe, under steady compression-sliding conditions, the relationship between fluid pressure p and volumetric strain ε_{vol} [23, 24].

$$\nabla \cdot \left(\frac{k}{\eta} \nabla p \right) = -\alpha \frac{D\varepsilon_{vol}}{Dt} \tag{6}$$

The left-hand-side term represents the pressure driven flow and the right-hand-side term describes the effect of compressing the material. In Eq. (6) k is the permeability, η is the fluid viscosity and α is the Biot-Willis coefficient. α describes the ratio of fluid volume squeezed into and out of the domain, therefore $\alpha = 1$ because the Poisson's ratio for the material is zero and all changes due to the material compressing must be accounted for by an equivalent change in the fluid phase.

The steady-state form for the fluid phase is described by Eq. (7), where $\mathbf{v}$ is the solid velocity of the rotating bodies. By implementing an Eulerian frame of reference $\mathbf{v}$ is subsequently given by Eq. (8) [18, 19], where for each body the centres of rotation are $x_{c,1} = 0, y_{c,1} = R_{1,o}$ and $x_{c,2} = 0, y_{c,2} = -R_{2,o}$. Additionally, under linear elastic assumptions the volumetric strain is defined as the divergence of the deformation field $\varepsilon_{vol} = \nabla \cdot \mathbf{u}$.

$$\nabla \cdot \left(\frac{k}{\eta} \nabla p \right) = -\alpha \mathbf{v} \cdot \nabla \varepsilon_{vol} \tag{7}$$

$$\mathbf{v} = \Omega \left(y - y_c, x - x_c \right) \tag{8}$$

In order to couple the fluid phase to the solid phase pressure gradients are implemented as a body force in the stress-strain relationship, leading to Eqs. (9)-(12) as based on Biot's theories for a zero Poisson's ratio material [25-27]. Note that in Eq. (2) the second term on the right-hand-side contains $\varepsilon_{vol} = \text{tr}(\boldsymbol{\varepsilon}) = \nabla \cdot \mathbf{u}$ which in Eq. (10) for the solid stress vanishes because for a poroelastic material volumetric strain instead causes a change in the fluid phase (Eq. (7)), which in turn has an effect on the equation of state for the solid phase (Eq. (9)). Based on these assumptions in a poroelastic material the solid stress therefore only describes the isochoric response of the structure, the response due to volumetric changes instead causes an equivalent change in the fluid pressure. The constitutive equations derived are similar to those which form biphasic theory for articular cartilage [13-17] and in general describe the poroelastic response of the material under load in an Eulerian frame of reference [18, 19].

$$\nabla \cdot \boldsymbol{\sigma} = \alpha \nabla p \tag{9}$$

$$\boldsymbol{\sigma} = 2\mu\boldsymbol{\varepsilon} \tag{10}$$

$$\boldsymbol{\varepsilon} = \frac{1}{2}\left[\nabla\mathbf{u} + (\nabla\mathbf{u})^{\text{T}}\right] \tag{11}$$

$$\mu = \frac{E}{2} \quad \lambda = 0 \tag{12}$$

Boundary conditions for the solid deformation in the poroelastic model are implemented using the same method as described in Section 2.1 for elastic contact. For the fluid flow a zero pressure condition $p = 0$ is applied to the extents of the contacting bodies, these locations are modelled to be far enough from the contacting region to assume that there is no change in fluid conditions. A zero flux condition $\mathbf{n} \cdot \left(\frac{k}{\eta}\nabla p\right) = 0$ is applied to the upper and lower surfaces of the bodies, this assumes that no fluid is transferred at the boundaries and the flow comes to rest (wall type condition). At the contacting interface this latter condition can be interpreted as no leakage between the bodies as they are compressed and as such mass is conserved. Models have been developed to explore the potential of a lubricating region along the contacting boundary in which flow in and out of the poroelastic material is permitted [18], however in this model no lubrication is assumed and fluid does not leave the contacting bodies.

The load carrying capacity of the poroelastic contact $F_{poroelastic}$ is given by Eq. (13) as the sum of two terms each representing the solid and fluid contributions respectively. The solid load F_{solid} is calculated from Eq. (5) and is identical to that of only contribution to load in elastic contact, the fluid load F_{fluid} is described by Eq. (14) as the integral of pressure over the contacting interface. This demonstrates the fundamental difference between elastic and poroelastic contacts whereby in the latter there is an additional contribution due to the presence of a fluid phase.

$$F_{poroelastic} = F_{solid} + F_{fluid} \tag{13}$$

$$F_{fluid} = \int p \, ds_1 + \int p \, ds_2 \tag{14}$$

3. Materials and Methods

This section outlines the selection of model parameters and materials used in order to model soft elastic and poroelastic contacts.

3.1 Model Parameters

In order to simulate soft elastic and poroelastic contacts the model parameters were chosen in order to reproduce typical conditions observed in biological systems such as articular cartilage found in mammalian joints. For the purpose of simplicity the geometry and material properties are kept the same for the two contacting bodies. The Young's modulus of the materials was considered over the range of E = 0.5 - 5 MPa which is several orders of

magnitude less than the materials used in hard mechanical bearings and gears (where $E > 100$ GPa). Therefore the elastic material modelled is considered soft and the poroelastic material modelled exhibits a similar magnitude of stiffness. For the soft elastic material a Poisson's ratio of almost $\nu = 0.5$ was assumed as to represent an incompressible solid. Simulations of soft elastic materials with $\nu = 0$ are also analysed, this represents the case of the poroelastic material without any fluid contribution. The fluid viscosity and permeability of the porous media were determined from papers investigating the material properties of synovial fluid and articular cartilage [28, 29]. The inner and outer radii of the contacting bodies were given values of 100 mm and 99 mm respectively, resulting in a 1 mm thickness for the cartilage layer. The size and thickness of the contacting bodies were chosen based on a survey of literature investigating the physiology of human joints and their operation, this also allowed the values of angular velocities to be established from a typical human walking cycle.

3.2 Solution Procedure

Both the elastic and poroelastic contact models were setup and solved using the computer software COMSOL Multiphysics [30]. For the poroelastic model this required the constitutive equations for each of the fluid and solid phases to be programmed into the software which subsequently applies the appropriate numerical discretisation, particular attention was needed in order to fully couple the Eulerian frame of reference used to define rotation of the solid bodies. The computational domain was discretised using 400 x 40 = 16000 quadrilateral elements for each body (32000 total elements), the spacing between elements was uniform in y and grown with increasing distance from the contact region in x. This mesh resolution was found to produce grid independent results for both models, with a < 1% change in the load carrying capacity observed from meshes with more than 32000 elements. For the range of simulations undertaken in Section 4 the minimum calculation time was 1 min 13 seconds and the maximum 4 mins 37 seconds, these were computed on a CPU with 4-core Intel-Xeon processors running at 3.3 GHz and 16 GB RAM.

Parameter	Value/Range [Unit]
Elastic Young's Modulus E	0.5 - 5 [MPa]
Elastic Poisson's ratio ν	0.4999
Poroelastic Young's Modulus E	0.5 - 5 [MPa]
Poroelastic Poisson's ratio ν	0
Outer Radii $R_{1,o}, R_{2,o}$	100 [mm]
Inner Radii $R_{1,i}, R_{2,i}$	99 [mm]
Angular Velocities Ω_1, Ω_2	1, -1 [rad/s]
Penetration Depth δ	-100 [µm]
Fluid Viscosity η	0.001 [Pa.s]
Permeability k	1×10^{-15} [m^2]
Biot-Willis Coefficient α	1

Table 1 – Material properties and operating conditions

4. Results and Discussion

Results are presented in this section investigating the differences between the performance of soft elastic and poroelastic contacts under load.

4.1 Soft Elastic Contact Simulations

Figure 2 presents an example of the von Mises' stress distribution in the soft elastic solid under load, for this result the indentation depth was selected as $\delta = -100$ µm, the Young's modulus as $E = 1$ MPa and Poisson's ratio as $\nu = 0.4999$. The von Mises's stress indicates the magnitude of the stress tensor such that larger values are closer to the yield point of the material. There is a concentration of higher stresses in the centre of the contacting region

than those toward the domain extents, demonstrating how stress due to the contact causes the material to deform such that there is no penetration of the bodies. The maximum von Mises' stress was found to be 59.7 kPa and was positioned in the centre of the contact (x = 0) on the opposite sides to the contacting interface (same for both bodies). Moving away from the centre of the contact, stress is reduced toward a minimum value before increasing and plateauing at the edge of the contact region, this analysis is useful in identifying the distribution of stress in a soft solid contact and further to compare with the poroelastic solutions presented in Section 4.2.
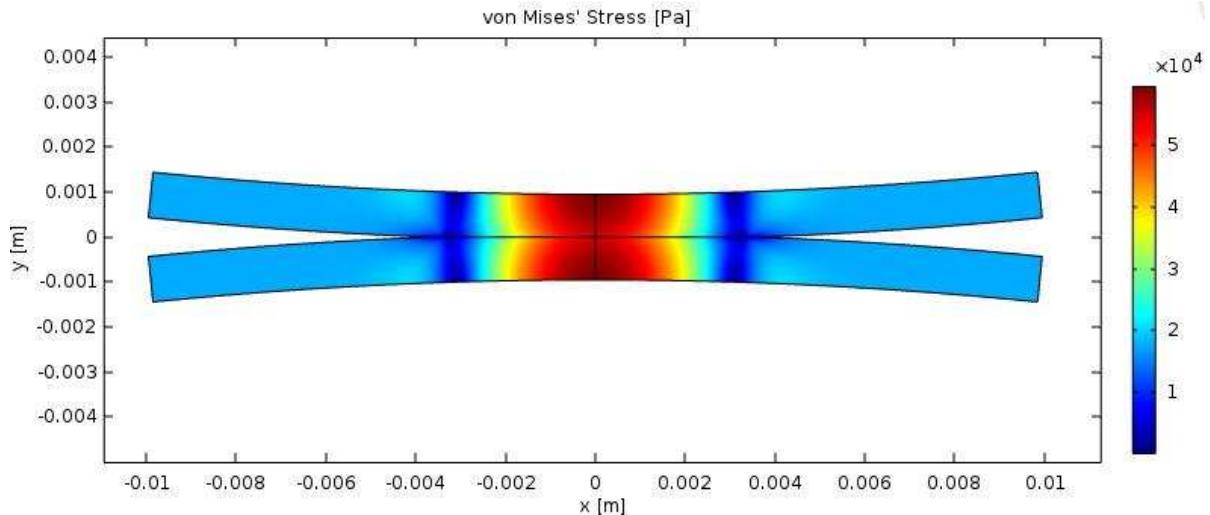

Figure 2 – von Mises' stress distribution in the soft elastic contact. E = 1 MPa, $\delta = -100$ μm.

4.2 Poroelastic Contact Simulations

Figures 3 and 4 respectively show examples of the von Mises's stress and pressure distributions in the poroelastic material under load. In these results the separation was selected as $\delta = -100$ μm and the poroelastic Young's modulus as E = 1 MPa. Concentrations of solid stress are observed in the contacting region and which decay with increasing distance from the centre of the contact, as was similarly shown for the soft elastic contact. Additionally, Figure 3 shows an increased magnitude and rate decay of solid stress with distance from the centre of the contact than that presented in Figure 2. The maximum von Mises' stress reached in the poroelastic material was 81.4 kPa which is significantly larger than the 59.7 kPa reached in the soft elastic material. This maximum was found to occur at the same location in both materials.The maximum and minimum pressures reached in the poroelastic material were found to be 51.6 kPa and -26.9 kPa, these were respectively located directly in the centre of the contacting region (x=0, y=0) and at the two locations where contact is onset. It is interesting to note the significant negative pressures reached in the contact, these are generated as a result of the contact stresses produced as the bodies penetrate. Fluid is moved as the solid body rotates into and out of the contact region, in order to maintain such and interface under contact conditions fluid is moved toward these negative pressure regions from the centre of the contact where pressure is largest.
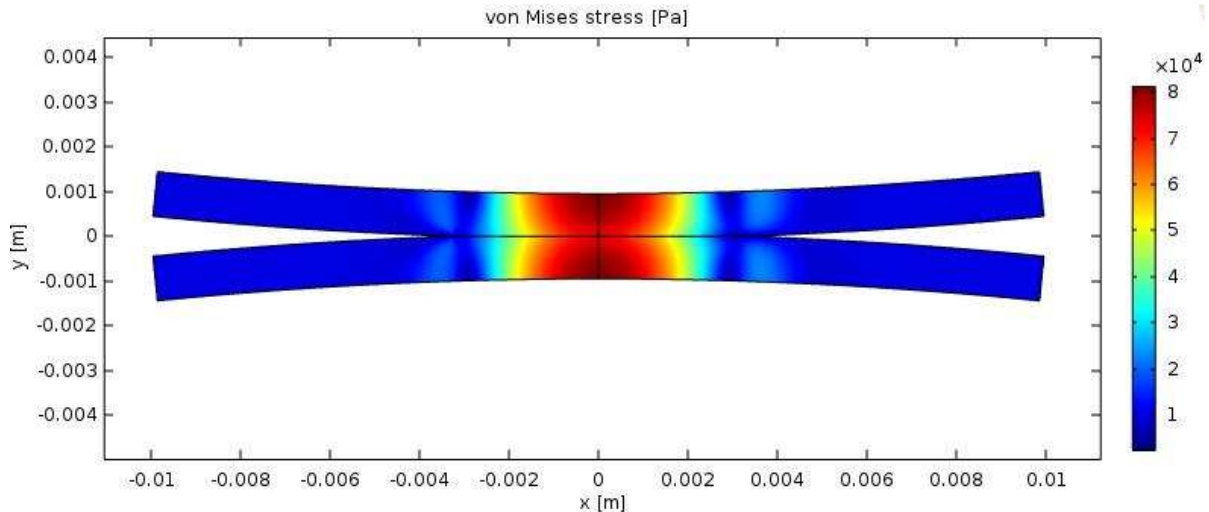
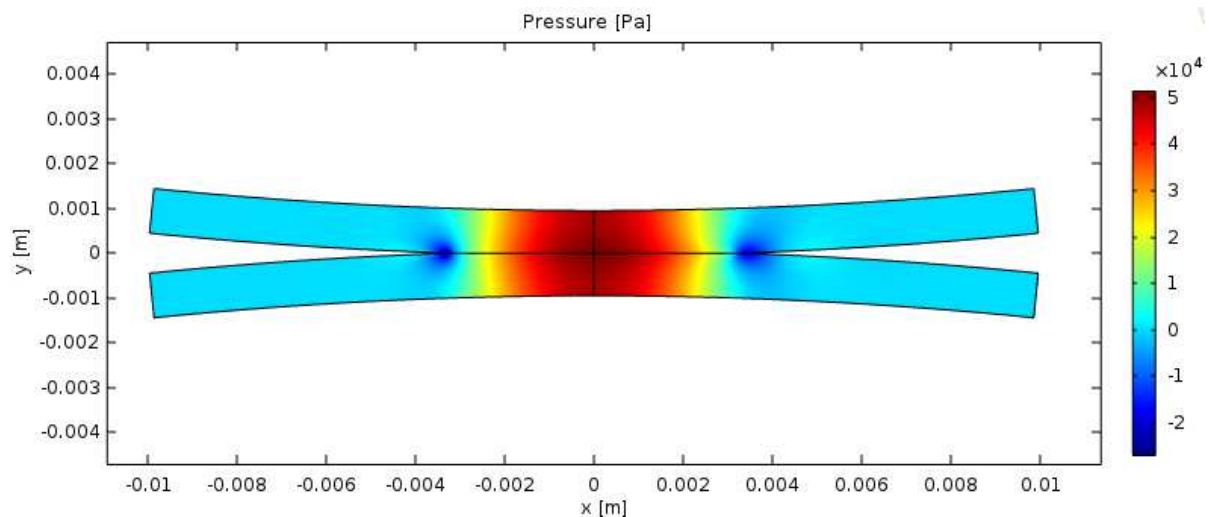Figure 3 - von Mises' stress distribution in the poroelastic contact. E = 1 MPa, $\delta = -100$ μm.

Figure 4 - Pressure distribution in the poroelastic contact. E = 1 MPa, $\delta = -100$ μm.

Figure 5 furthers this analysis by presenting the poroelastic fluid pressure and contact pressure along the length of the contacting interface, also given is the contact pressure for the soft elastic solid. Under purely elastic conditions a typical Hertzian type distribution is given for the contact pressure, which is symmetrical in shape about the centre of the contact. In the poroelastic case neither the contact pressure nor fluid pressure are symmetric and overall the contact area (the region in which the contact pressure is positive) is larger. This asymmetry relates to non-linearity introduced by the rotating frame of reference in the poroelastic model, as material is deformed into and out of the contact the poroelastic material responds by moving fluid.

Authors have demonstrated that poroelastic materials are capable of very low friction due to their biphasic nature [7-11, 13-17], and the results presented in this section describe some the mechanisms by which this is achieved. However fluid flow is not permitted into or out of the material in this model, under flooded conditions this could be a possible means for even further improvements to the tribology of the system. Experiments have identified the benefit of such flows in cartilage which boost the lubrication performance, recently this has been referred to as tribological rehydration [9-11]. This model indicates the potential means by which this is facilitated, in which flow across the contacting interface would be permitted and lubrication theory used to govern fluid flow outside the contact [18].
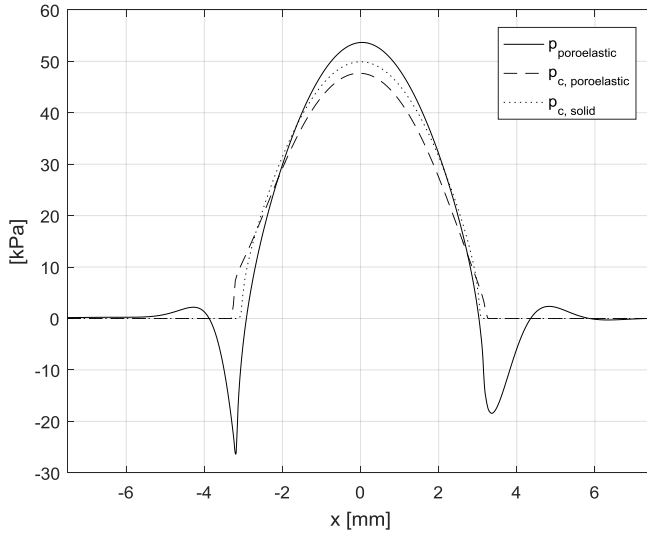
7

Figure 5 – Comparison of the poroelastic fluid pressure, poroelastic contact pressure and solid contact pressure along the interface between the rotating bodies. E = 1 MPa, δ = −100 μm.

4.3 Load Carrying Capacity

In order to demonstrate the difference between the load carrying capacity of soft elastic and poroelastic contacts the separation δ was parametrically varied between 0 and -100 μm, the resulting values of $F_{elastic}$ at ν = 0.5, $F_{elastic}$ at ν = 0 and $F_{poroelastic}$ are presented in Figure 6. For this analysis the Young's modulus was chosen as E = 1 MPa for all cases. Figure 6 indicates that the poroelastic contact carries less load than the soft elastic contact at ν = 0.5 for any given separation, or in other words to achieve the same load the poroelastic material must deform more than the soft elastic material. This shows that in poroelastic materials the presence of interstitial fluid in the pores of the solid structure causes a greater resistance to load than found in soft elastic solids with ν = 0.5. It is also shown that the contribution of the solid and fluid phases to the total load capacity of the poroelastic contact are almost equal because the load given by the elastic material with ν = 0 is half that of the poroelastic case, which itself represents the exact same solid response with an additional contribution due to fluid pressure. Further to this, and given the results presented in Section 4.2, as the poroelastic material must deform more to carry the same load the corresponding peak solid stress will be higher than that found in the soft elastic material with ν = 0.5 under the same conditions. These results coincide with the findings of articles published exploring the biphasic nature of cartilage, in which it is known that the material must deform more to carry the same load as an elastic material with an equivalent stiffness [15-18].
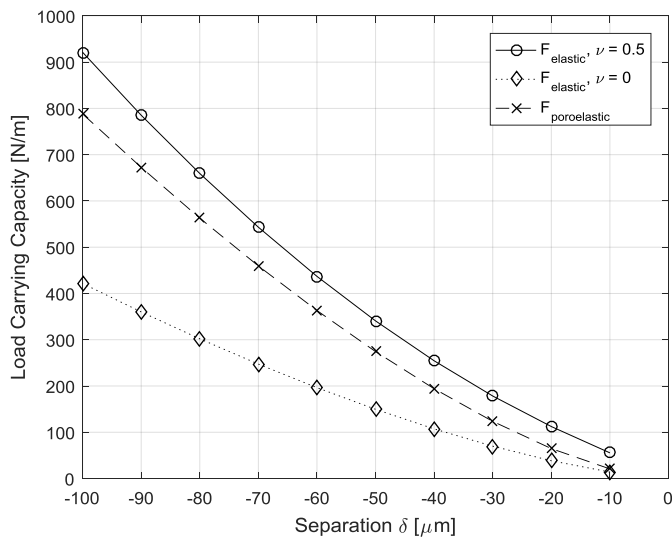
Figure 6 – Comparison of the load carrying capacity of soft elastic and poroelastic as a function of the separation between the contacting bodies. E = 1 MPa.

4.4 Effect of Young's Modulus

In this section the effect of varying Young's modulus on the load carrying capacity is investigated, this is undertaken for the soft elastic materials with $\nu = 0, 0.5$ and the poroelastic material over a range of $E = 0.5 - 5$ MPa. A separation of $\delta = -100$ μm was chosen for this study. Figure 7 demonstrates that increasing the Young's modulus leads to a linear increase in the load for all cases, the rate of increase is larger for the soft elastic material with $\nu = 0.5$ than for the poroelastic material, the difference between the two loads is also shown to increase with E. This result indicates that the Young's modulus scales the stiffness of the load-deformation response and that, for any given separation, the soft elastic material with $\nu = 0.5$ carries more load than the poroelastic material. This further implies that for the poroelastic material to hold the same load as the soft elastic material with $\nu = 0.5$ at any given separation, the Young's modulus must take a larger value and that therefore the solid structure would therefore be stiffer. The Young's modulus is also shown to not change the ratio of solid and fluid contributions to the total load carrying capacity of the poroelastic contact, that is where the elastic material with $\nu = 0$ gives half the load capacity of the poroelastic material for all values of E. Additionally, it is seen that reducing the Poisson's ratio toward zero for a solid material has the effect of reducing the load for any given depth. This is an interesting effect similar to that observed when modelling the presence of an interstitial fluid in the poroelastic material. This demonstrates findings similar to articles investigating biphasic theory [15-18] in which an increase in load with stiffness is exhibited and that this differs significantly to those predictions made for soft elastic materials.
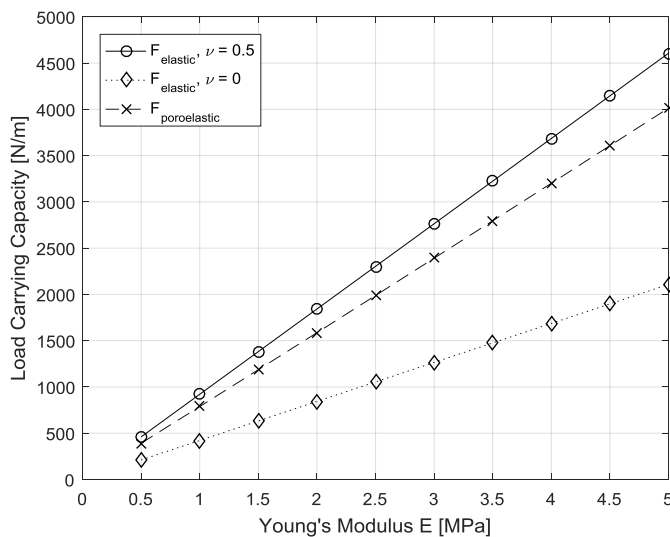

Figure 7 – Effect of Young's modulus on the load carrying capacity of soft elastic and poroelastic materials in contact. $\delta = -100$ μm.

5. Conclusion

In this paper computational models for the contact of soft elastic and poroelastic bodies rotating under load were developed and used to investigate differences in the load carrying capacity exhibited between the two types of material. The parameters used were chosen to represent human joints in operation, where both types of material have been previously employed to investigate biological tribology as a means to simulate the interactions observed in practice. For the models developed steady-state conditions were imposed and the rotational velocities of the bodies were considered in an Eulerian frame of reference, this led to the assumption of steady compressing-sliding at the contacting interface. Linear elasticity was used to describe the structural solid behaviour of both materials. The soft elastic material was assigned a Poisson's ratio of almost $\nu = 0.5$ which is a well-established approach for modelling biological materials under load. The poroelastic material was defined using Biot's theories in which the Poisson's ratio was set to zero and all changes due to volumetric strain caused an equivalent change in the fluid pressure as described by Darcy's law. The load carrying capacity of the two types of contact was subsequently investigated, for the soft elastic material only solid stress generated load whereas in contrast in the poroelastic material both solid stress and fluid pressure contributed to the load carrying capacity.

Results presented showed that a more negative value of the separation between the contacting bodies led to a monotonic increase in the load, this applied to both cases investigated with the soft elastic material with $\nu = 0.5$ capable of carrying more load than the poroelastic material at any given separation. This further implied that to carry the same load the poroelastic material must deform further than the soft elastic material with $\nu = 0.5$, this potentially explains how poroelastic materials operate in biological systems by deforming more than would be expected due to the presence of a fluid phase, as is consistent with papers investigating biphasic theory [15-18]. An increase in the Young's modulus of both types of material was shown to scale the load carrying capacity at any given separation, this demonstrated how the Young's modulus changes the stiffness of the solid structure and therefore the load which can be carried in the contact, which is again in line with biphasic theory [15-18]. Additionally, it was shown that the solid and fluid contributions to load in the poroelastic material were equal and independent of the separation and solid stiffness. Visualisation of the solid stress and fluid pressure distributions generated in the poroelastic material under load demonstrated that in order to maintain the interface between the bodies fluid is moved from the centre of the contact toward the regions where contact is onset. It was also shown that in a poroelastic material the solid stresses generated in the contact are large than those observed in soft solid contacts under the same condition, this is interesting to note given the presence of an interstitial fluid which carries part of the poroelastic load.

Overall this paper highlights the differences between soft elastic materials and poroelastic materials when they come into contact while rotating under load. Due to the difference between how load is carried there is a fundamental change to how the materials respond when deformed, for poroelastic materials this could explain in biological systems how large deformations can be observed for reasonable loads which cannot be described without the biphasic approach. Further development of this model will include the addition of lubrication at the contacting interface and elastohydrodynamic effects to be incorporated into the poroelastic model, this will allow the analysis of dry contacts as explored here to be expanded to flooded conditions. Large deformations expected in biological systems will require hyperelasticity to describe the structural behaviour of the material, this would further the applicable range of parameters over which the biphasic model can accurate simulate such phenomena.

Acknowledgements

References

1. Neville A, Morina A, Liskiewicz T, Yan Y (2007). "Synovial joint lubrication – does nature teach more effective engineering lubrication strategies?" Proc IMechE Part C, 221: 1223-1230.
2. Forster H, Fisher J (1996). "The influence of loading time and lubricant on the friction of articular cartilage," Proc IMechE Part H, 210: 109-119.
3. Ateshian GA, Hung CT (2006). "The natural synovial joint: properties of cartilage," Proc IMechE Part J, 220: 657-670.
4. Ferguson SJ, Bryant JT, Ganz R, Ito K (2000). "The acetabular labrum seal: a poroelastic finite element model," Clinical Biomechanics, 15(6): 463-468.
5. Mansour JM (2003). "Biomechanics of cartilage," In: Oatis CA (ed.) Kinesiology: the mechanics and pathomechanics of human movement. Philadelphia, PA: Lippincott Williams & Wilkins, ch. 5, pp. 66-79.
6. McCutchen CW (1962). "The frictional properties of animal joints." Wear, 5:1-17.
7. Armstrong CG, Lai WM, Mow VC (1984). "An analysis of the unconfined compression of articular-cartilage." J Biomech Eng Asme, 106(2): 165-173.
8. Krishnan R, Kopacz M, Ateshian GA (2004). "Experimental verification of the role of interstitial fluid pressurization in cartilage lubrication." J Orthrop Res, 22: 565-570.
9. Bonnevie ED, Baro V, Wang L, Burris DL (2011). "In-situ studies of cartilage microtribology: roles of speed and contact area," Tribol Lett, 41(1): 83-95.
10. Moore AC, DeLucca JF, Burris DL, Elliot DM (2015). "Quantifying cartilage contact modulus, tensile modulus, and permeability with Hertzian biphasic creep," J Tribol, 138(4): 041405-1-7.
11. Moore AC, Burris DL (2017). "Tribological rehydration of cartilage and its potential role in preserving joint health," Osteoarthritis and Cartilage, 25: 99-107.
12. Biot MA (1962). "Mechanics of deformation and acoustic propagation in porous media," Journal of Applied Physics, 33(4): 1482-1498.

13. Mow VC, Kuei SC, Lai WM (1980). "Biphasic creep and stress-relaxation of articular-cartilage in compression – theory and experiments." J Biomech Eng Asme, 102(1): 73-84.
14. Mow VC, Holmes MH, Lai WM (1984). "Fluid transport and mechanical properties of articular cartilage: a review. J Biomech, 17(5): 377-394.
15. Ateshian GA, Wang HQ (1995). "A theoretical solution for the frictionless rolling-contact of cylindrical biphasic aricular cartilage layers. J Biomech, 28(11): 1341-1355.
16. Caligaris M, Ateshian GA (2008). "Effects of sustained interstitial fluid pressurization under migrating contact area, and boundary lubrication by synovial fluid on cartilage friction." Osteoarthritis and Cartilage, 16(10): 1220-1227.
17. Ateshian GA, Maas S, Weiss JA (2010). "Finite element algorithm for frictionless contact of porous permeable media under finite deformation and sliding." J Biomech Eng, 132(6): 061006.
18. Hu R, Hewson R, Morina A, Liu Z (2014). "Influence of material properties and operating conditions on the predicted performance of poroelastic faced bearings," Proc IMechE Part J, 228(2): 131-139.
19. Simon BR (1992). "Multiphase poroelastic finite element models for soft tissue structures." Appl Mech Rev, 45(6): 191–218.
20. Benham PP, Crawford RJ, Armstrong CG (1996). "Mechanics of engineering materials," 2nd Ed., Pearson, Harlow, UK.
21. Mott PH, Dorgan JR, Roland CM (2008). "The bulk modulus and Poisson's ratio of "incompressible" materials." J Sound and Vibration, 312(4): 572-575.
22. Johnson KL (1987). "Contact mechanics," Cambridge University Press, Cambridge, UK.
23. Preziosi L, Farina A (2002). "On Darcy's law for growing porous media," Int J Non-Linear Mech, 37(3): 485-491.
24. Pan R (2006). "Darcy's law as long-time limit of adiabatic porous media flow," J Differen Equat, 220(1): 121-146.
25. Biot MA (1941). "General theory of three-dimensional consolidation," J Appl Phys, 12(2): 155-164.
26. Biot MA (1955). "Theory of elasticity and consolidation for porous anisotropic solid," J Appl Phys, 26(2): 182-185.
27. Biot MA (1956). "General solutions of the equations of elasticity and consolidation for a porous material," Appl Mech, 78: 91-96.
28. Jin ZM, Pickard JE, Forster H, Ingham E, Fisher J (2000). "Frictional behaviour of bovine articular cartilage," Biorheology, 37(1-2): 57-63.
29. Warner MD (2000). "Finite element biphasic modelling of articular cartilage: An investigation into crystal induced damage," PhD Thesis, University of Bath, UK.
30. COMSOL Inc. (2017). COMSOL Multiphysics v5.2a [Computer Software]. Retrieved from http://www.comsol.com/.